PHYSICAL REVIEW B **92**, 020503(R) (2015)

Two-dimensional superconductor-insulator quantum phase transitions in an electron-doped cuprate

S. W. Zeng,[1,2] Z. Huang,[1] W. M. Lv,[1] N. N. Bao,[1,3] K. Gopinadhan,[1] L. K. Jian,[1] T. S. Herng,[3] Z. Q. Liu,[4] Y. L. Zhao,[1] C. J. Li,[1] H. J. Harsan Ma,[1,2] P. Yang,[5] J. Ding,[1,3] T. Venkatesan,[1,2,6,*] and Ariando[1,2,*]

[1]*NUSNNI-NanoCore, National University of Singapore, Singapore 117411*

[2]*Department of Physics, National University of Singapore, Singapore 117542*

[3]*Department of Materials Science and Engineering, National University of Singapore, Singapore 117576*

[4]*Oak Ridge National Laboratory, Oak Ridge, Tennessee 37831, USA*

[5]*Singapore Synchrotron Light Source (SSLS), National University of Singapore, 5 Research Link, Singapore 117603*

[6]*Department of Electrical and Computer Engineering, National University of Singapore, Singapore 117576*

(Received 21 May 2014; revised manuscript received 3 June 2015; published 6 July 2015)

We use an ionic liquid-assisted electric-field effect to tune the carrier density in an electron-doped cuprate ultrathin film and cause a two-dimensional superconductor-insulator transition (SIT). The low upper critical field in this system allows us to perform magnetic-field (B)-induced SIT in the liquid-gated superconducting film. Finite-size scaling analysis indicates that SITs induced both by electric and by magnetic fields are quantum phase transitions and the transitions are governed by percolation effects—quantum mechanical in the former and classical in the latter cases. Compared to the hole-doped cuprates, the SITs in the electron-doped system occur at critical sheet resistances (R_c) much lower than the pair quantum resistance $R_Q = h/(2e)^2 = 6.45\,\mathrm{k\Omega}$, suggesting the possible existence of fermionic excitations at finite temperatures at the insulating phase near the SITs.

DOI: 10.1103/PhysRevB.92.020503 PACS number(s): 74.25.Dw, 74.25.F−, 74.40.Kb, 74.72.Ek

Electric-field-effect doping has long been a key technology to tune the charge carrier of a material in a reversible quasicontinuous way and without inducing structural changes [1–5]. More recently, the field effect in a electronic double-layer transistor (EDLT) configuration which uses ionic liquids (ILs) and a polymer electrolyte as gate dielectrics has been shown to induce a large amount of carriers (up to a level of $10^{15}/\mathrm{cm}^2$) at the surface of a thin film [6] and thus is attracting growing interest. The capability of EDLTs in accumulating charge carriers has been demonstrated by gate-induced phase transitions in various materials [6–18]. In particular, employing EDLT superconductivity has been induced in nonsuperconducting samples, such as $SrTiO_3$ [7], $KTaO_3$ [9], ZrNCl [8], MoS_2 [15], and the hole-doped cuprate $La_{2-x}Sr_xCuO_4$ (LSCO) [11].

Tuning the carrier density in high-T_c cuprates is of particular interest since the properties of cuprates depend dramatically on the charge carriers. Doping both holes and electrons could cause the change in cuprates from antiferromagnetic Mott insulators to high-T_c superconductors. However, what happens near the critical point where superconductor-insulator transition (SIT) occurs, and what are the differences between hole- and electron-doped cuprates at the critical point are key open questions. To address such questions, quasicontinuous tuning of carrier density by electric-field effect across the SIT point is required. In the hole-doped cuprates LSCO and $YBa_2Cu_3O_{7-x}$ (YBCO), EDLT-tuned two-dimensional (2D) SIT occurred at pair quantum resistance $R_Q = 6.45\,\mathrm{k\Omega}$ [11,12], which suggests that Cooper pairs preserve at both superconducting and insulating sides near the SIT as opposed to the formation of fermionic excitations. Furthermore, it has been suggested that the SITs in a hole-doped system are 2D quantum phase transitions (QPTs) via finite-size scaling analysis. However, a counterpart of LSCO, electron-doped $R_{2-x}Ce_xCuO_4$ (R = Pr, Nd, Sm, or Eu) exhibits different crystalline structures, phase diagrams, and electronic properties [19]. These suggest that the SITs in electron-doped cuprates may be expected to be different. Understanding the nature of carrier-induced SITs in electron-doped systems should shed more light on the origins of superconductivity in cuprates.

Furthermore, as the SIT strongly depends also on the dynamics of the vortices, it would be revealing if a B-induced SIT could be studied as one suppresses the superconductivity via vortices as opposed to charge injection. B-induced SITs in cuprates have been investigated in chemically doped superconductors [20,21]. Unlike chemical doping, superconductivity induced by an EDLT has a distinct 2D nature due to the short screening length in cuprates [11,22]. B-induced SIT in such an EDLT superconducting state would be very interesting. However, this has not been performed in hole-doped cuprates due to the huge upper critical field H_{c2}. In electron-doped cuprates H_{c2} is much lower, and this provides an opportunity to study a B-induced SIT in a superconducting EDLT.

In this Rapid Communication, we simultaneously study the SITs induced by both electric and magnetic fields in electron-doped $Pr_{2-x}Ce_xCuO_4$ (PCCO) ultrathin films. Using the EDLT configuration, electrostatically induced superconducting transition in an initially insulating PCCO ultrathin film is observed. In such superconducting EDLTs with different doping levels, insulating states are realized by applying magnetic fields. We found that the SITs induced by both electric and magnetic fields occurred at R_c much lower than R_Q. Moreover, finite-size scaling analysis is performed, and it is suggested that the transitions are 2D-QPTs.

Ultrathin layering structures with nominal 1 unit cell (uc) underdoped PCCO on 4-uc Pr_2CuO_4 (PCO) were grown on TiO_2-terminated $SrTiO_3$ (001) substrates by a pulsed laser deposition (PLD) system. The Ce contents of the top $Pr_{2-x}Ce_xCuO_4$ layers are $x_{Ce} = 0.1$ (samples A and B) and

*Author to whom correspondence should be addressed: venky@nus.edu.sg and ariando@nus.edu.sg

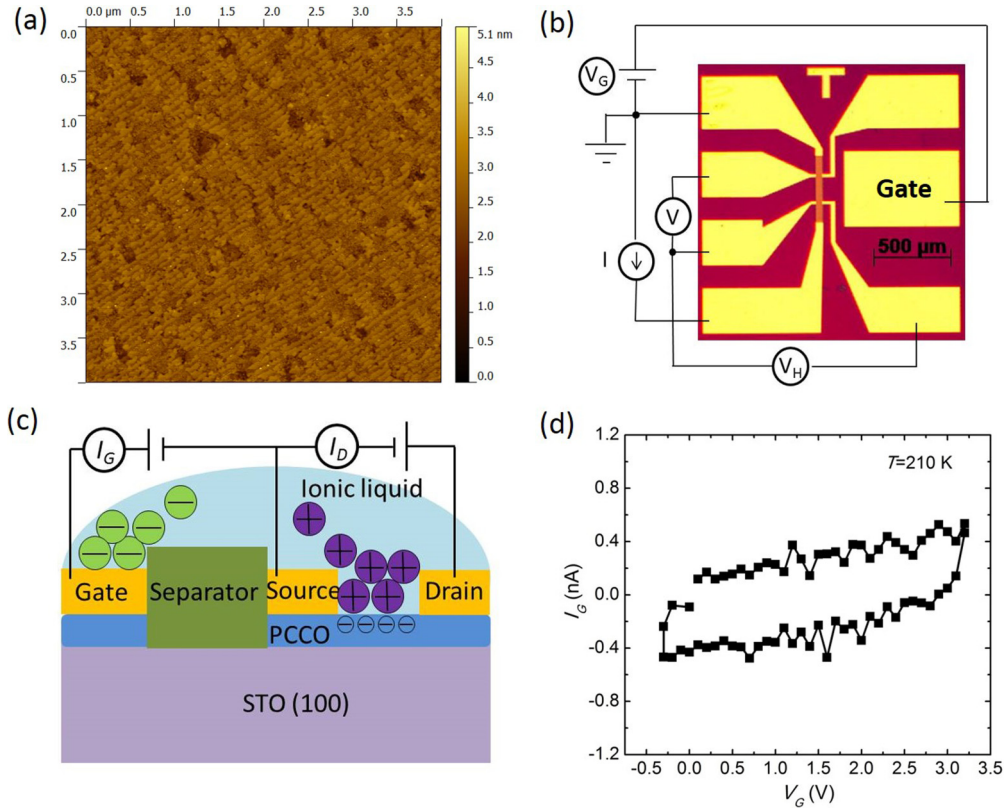

FIG. 1. (Color online) (a) Atomic force microscopy image ($4 \times 4\ \mu m^2$) of the surface of ultrathin PCCO/PCO films. (b) Optical micrograph of a typical device and the measurement circuit. (c) Schematic of the operation of an EDLT. (d) Gate voltage (V_G) dependence of the leakage current (I_G).

0.04 (sample C). The thin films were deposited at 790 °C under an oxygen partial pressure (P_{O_2}) of 0.25 mbar and then cooled down to room temperature from 720 °C in vacuum ($P_{O_2} < 10^{-4}$ mbar) at a cooling rate of 20 °C/min. Figure 1(a) shows an atomic force microscopy image of ultrathin PCCO/PCO films. The root-mean-square roughness is ~0.32 nm, indicating a smooth surface of thin films. Devices with a Hall bar geometry were fabricated to accurately measure the sheet resistance. Before deposition of thin films, $SrTiO_3$ substrates were patterned into Hall bar geometry by using conventional photolithography and depositing amorphous AlN films as hard masks. Then, the patterned substrates were set into a PLD chamber for the deposition of the thin films. Finally, after film deposition, Cr/Au (10/70 nm) layers were deposited for current/voltage probes and gate electrodes. A micrograph of a fabricated device is shown in Fig. 1(b). The width of the Hall bar is 50 μm, and the length is 500 μm. A six-probe configuration of the Hall bar allows for the measurement of both longitudinal and Hall resistances. A large planar gate electrode is used to accumulate ions.

A small droplet of the IL, *N*,*N*-diethyl-*N*-methyl-*N*-(2-methoxyethyl) ammonium bis(trifluoromethyl sulphonyl)imide, covered both the conducting channel and the gate electrode. Then the sample was set into the chamber of a Quantum Design physical property measurement system for the transport measurements. The gate voltage (V_G) was applied at 210 K and kept for 20–40 min for charging. A resistance measurement was made as the samples were cooled down while keeping the V_G constant. In order to change V_G, the sample was heated to 210 K after each resistance-temperature curve measurement and a new V_G was applied. As is shown in Fig. 1(c), when a positive V_G is applied, the mobile cations accumulate on the transport channel and induce electrons on the surface of the thin film. Figure 1(d) shows the leakage current (I_G) as a function of V_G for a PCCO-EDLT device. It can be seen that I_G is on the order of 1 nA. This negligibly small I_G indicates good operation of the device. In these experiments the IL predominantly induces charges at the surface as opposed to changing the local oxygen vacancy concentration [17,23].

Figures 2(a) and 2(b) show the sheet resistance versus temperature ($R_s - T$) curves at various V_G's for samples with $x_{Ce} = 0.1$ (sample A) and $x_{Ce} = 0.04$ (sample C). The $R_s - T$ curves of sample B can be seen in the Supplemental Material Fig. S8 [24]. Since the Ce content is lower in sample C, initial resistance at $V_G = 0$ V is much higher than that of sample A. Many curves were recorded, and insulator-to-superconductor transitions were observed in both of the samples. The initially underdoped samples show insulating behavior. Even at the V_G near the SIT, the resistance increases with decreasing T below ~140 K, suggesting that EDLT samples have a much higher resistance at the insulating phase (Supplemental Material Sec. 6 [24]). As V_G is increased, the accumulation of electrons on the surface is enhanced, and the R_s decreases. Note that the bottom PCO layer does not contribute to this resistance drop as verified by direct field-effect experiments on PCO without a top PCCO layer. At V_G above certain values (2.59 V

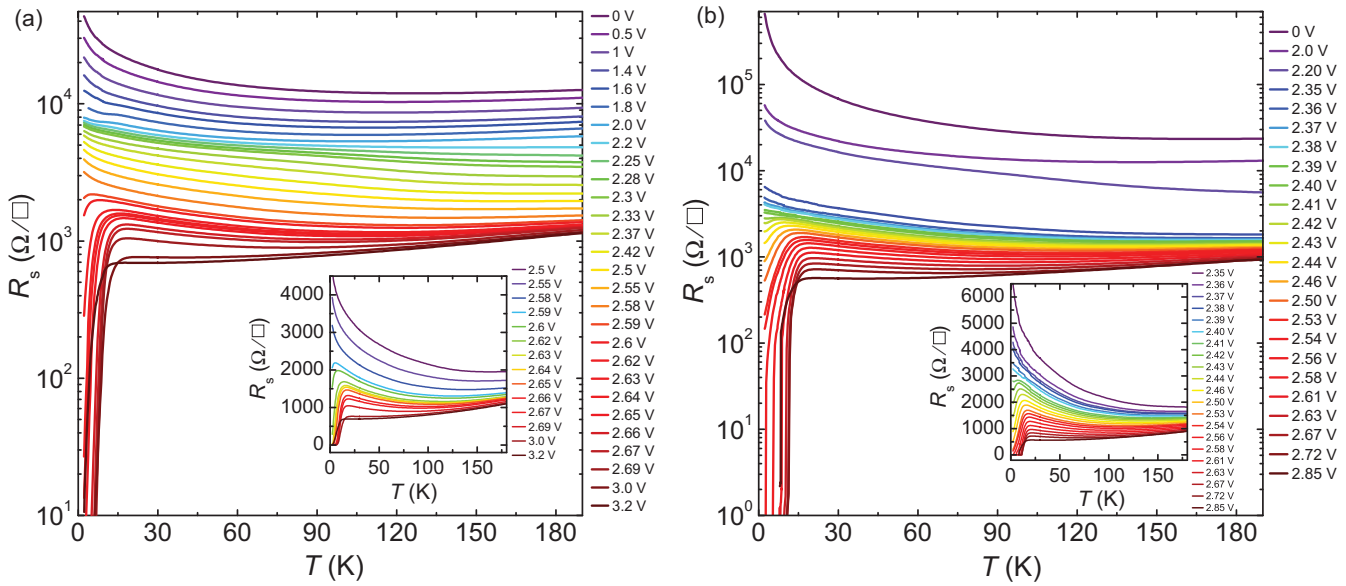

FIG. 2. (Color online) The logarithmic-scale sheet resistance versus temperature ($R_s - T$) curves at various V_G's for samples with Ce contents of (a) $x_{Ce} = 0.1$ (sample A) and (b) $x_{Ce} = 0.04$ (sample C). The insets are the linear-scale $R_s - T$ curves near the SITs.

for sample A and 2.41 V for sample C), the resistance drops sharply at low T, signaling the onset of superconductivity. As V_G is increased, the T_c increases up to a maximum of ∼14 K and then decreases for further increasing V_G. The T_c is taken to be the T at which the R_s falls to 50% of its normal-state value. Due to the short Thomas-Fermi screening length in cuprates [11,22], the active layer in the EDLT is limited to one or two CuO_2 planes, leaving the deeper layers unaffected. To further demonstrate this screening effect, devices with optimally doped $Pr_{1.85}Ce_{0.15}CuO_4$ showing superconducting T_c of ∼15 K were fabricated and tested. It was found that even at a higher V_G of 4 V, only a small change in T_c but no insulating phase was obtained in a film with thickness above 3 uc, indicating the shunting effect from the deeper layers which are not influenced by the field effect. These suggest that the superconductivity obtained in the underdoped EDLT devices occurs within one or two CuO_2 layers on the surface and, thus, is two dimensional. This is different from the multilayers of electron-doped cuprates in which the redistribution of charge could be over a long distance, and thus, the transport properties of one layer could be affected by the other ones [25].

The electric-field-effect-induced phase diagram of T_c versus carrier concentration x is constructed based on the measured R-T curves at different V_G's and shown in Fig. 3. The details of the estimation of x can be seen in the Supplemental Material Sec. 3 [26]. For comparison, a field-effect-induced phase diagram of hole-doped LSCO is extracted from Ref. [11] and plotted. The superconductivity occurs at doping levels of $x \approx 0.12$ for sample A and $x \approx 0.11$ for samples B and C, comparable to that in chemically doped PCCO [27]. These doping levels are much higher than that of LSCO, indicating that more charge carriers are required to induce superconductivity in electron-doped cuprate EDLT. This could also be seen from the fact that the V_G at which superconductivity occurs in PCCO (above 2 V) is higher than that (1.25 V) in LSCO [11]. The inset of Fig. 3 shows the normalized T_c, T_c/T_c ($x = 0.15$) as a function of x for field-effect and chemical dopings [27]. One can see that the phase diagrams derived from field-effect and chemical dopings are reasonably similar. This suggests that the estimation of x is reliable, a necessity for quantitative analysis near the SIT. The highest T_c obtained by field-effect doping is ∼14 K, which is lower than that of LSCO (∼29 K), and that (∼21 K) obtained by chemical doping [27]. The difference in T_c between EDLTs and chemically doped samples has also been observed in hole-doped LSCO [11]. This may be due to the possible disorder in the ultrathin film as well as the 2D nature of superconducting EDLTs.

It is proposed that the SIT at the limit of zero T and 2D is an example of a QPT [28–31]. At nonzero T, the signature of a QPT is a success of finite-size scaling in describing the finite-T data [2,11,12,28–34]. For a 2D system, the R_s near a quantum critical point collapses onto a single scaling function $R_s(x_t, T) = R_c F(|x_t - x_c|T^{-1/\nu z}$, where T is the temperature,

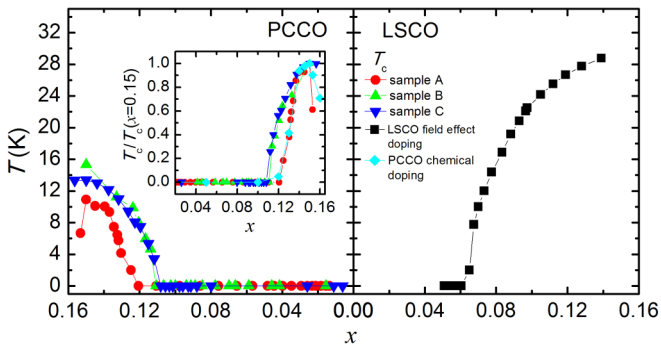

FIG. 3. (Color online) Electric-field-effect-tuned critical temperature T_c versus carrier concentration x for electron-doped PCCO (samples A–C) and hole-doped LSCO. T_c versus x for LSCO is extracted from Ref. [11]. The inset shows the normalized T_c, $T_c/T_c(x = 0.15)$ as a function of x for the electric-field-effect and chemical dopings. $T_c/T_c(x = 0.15)$ versus x for chemical doping of PCCO is extracted from Ref. [27].

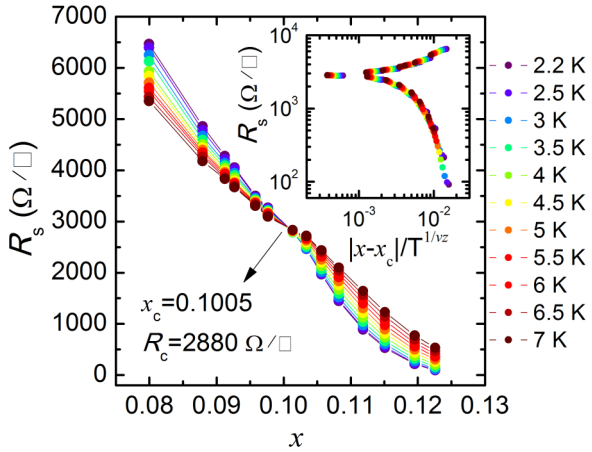

FIG. 4. (Color online) Isotherms of R_s as a function of x at T ranging from 2.2 to 7 K for sample C. The inset is the finite-size scaling of the isotherm curves, showing the resistance as a function of $|x - x_c|/T^{1/\nu z}$ with a critical exponent $\nu z = 2.4$.

x_t is the tuning parameter (in the present result, x_t is the carrier concentration and magnetic field), x_c is x_t at the critical point, R_c is the critical R_s at $x_t = x_c$, ν is the correlation length critical exponent, z is the dynamic critical exponent, and $F(u)$ is a universal function of u with $F(u) \to 1$ when $u \to 0$. The low-T resistances near the SIT were extracted for quantitative analysis. Figure 4 shows the resistance isotherms of sample C from 2.2 to 7 K as a function of x. One can see that all curves cross at a single point which separates the insulating and superconducting regimes. The data at the point give the critical values of x and R_s to be $x_c \approx 0.1005$ and $R_c \approx 2.88\,\mathrm{k}\Omega$. The R_c is much lower than R_Q. The inset of Fig. 4 is the finite-size scaling analysis of the data in the vicinity of the SIT. Given the exponent product $\nu z = 2.4$, all of the isotherm curves collapse onto a single function, suggesting the occurrence of a 2D-QPT. The scaling analysis of other samples is shown in the Supplemental Material Figs. S7–S9 [24], and the similar values of R_c and νz are also observed, indicating that our results are reproducible. The value of νz for PCCO is different from those for the hole-doped 214-structure counterpart, $\nu z = 1.5$ for LSCO [11] and $\nu z = 1.2$ for $La_2CuO_{4+\delta}$ [13]. It is consistent with that of the quantum percolation model ($\nu z \approx 7/3$) [12,35–38].

Magnetic-field (B)-tuned SITs were performed on sample A at three different V_G's of 2.75, 3.0, and 3.2 V, which correspond to underdoped, optimally doped, and overdoped states, respectively. At each V_G the sample was initially superconducting and could be tuned to insulating states (Supplemental Material Fig. S6 [24]). Figures 5(a)–5(c) show the R_s as a function of B at four T points below the onset of superconductivity. At each doping level, isotherms of R_s cross each other at a single point which separates the insulating from the superconducting phase. The critical magnetic fields B_c and

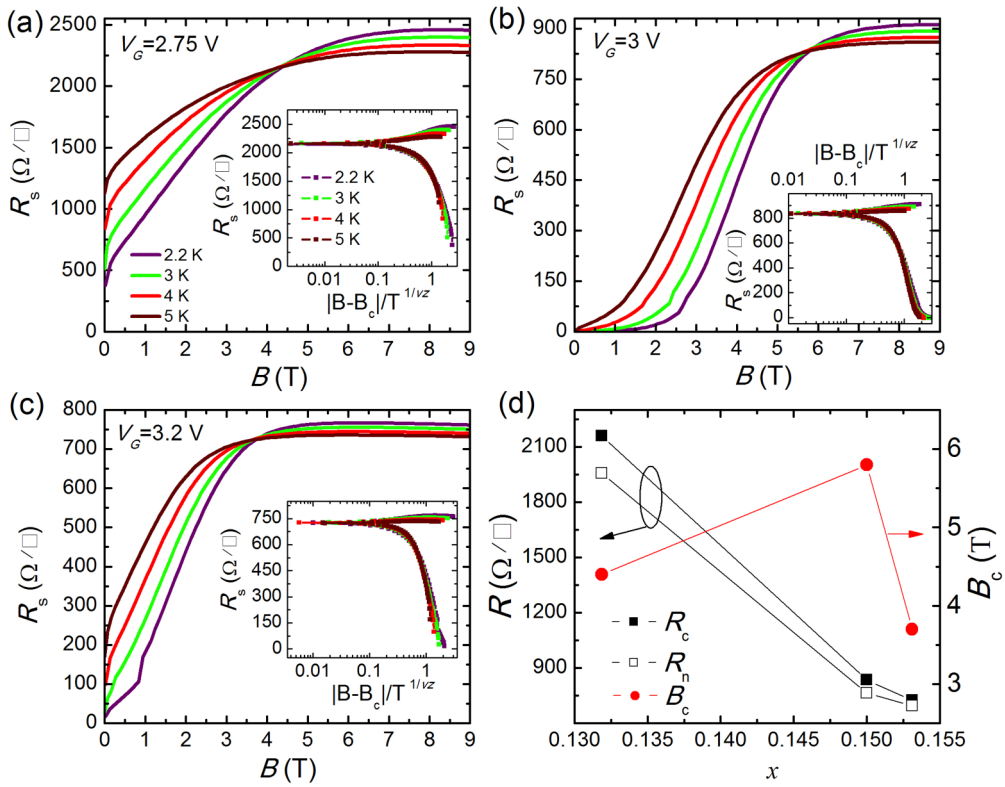

FIG. 5. (Color online) Resistances of sample A as a function of magnetic fields B at (a) $V_G = 2.75$ V, (b) $V_G = 3.0$ V, and (c) $V_G = 3.2$ V, corresponding to underdoped, optimally doped, and overdoped states ($x = 0.132$, 0.15, and 0.153), respectively. The insets show the R_s as a function of $|B - B_c|/T^{1/\nu z}$. The data can be fitted by a finite-size scaling function assuming $\nu z = 1.4$ for three doping levels. (d) R_c, R_n, and B_c, as a function of x which correspond to different V_G's. R_c and B_c are the resistances and magnetic fields at the points where the resistance isotherms cross each other. R_n is the resistance obtained at the onset of superconductivity and zero magnetic field (Supplemental Material Fig. S6(a) [24]).

R_c as a function of x are shown in Fig. 5(d). It can be seen that B_c peaks at the optimally doped state and shows lower values at underdoped and overdoped states. R_c is similar to R_n at each doping level, decreases with increasing doping levels, and is much lower than R_Q, especially for the ones at optimally doped and overdoped states. The insets of Figs. 5(a)–5(c) show a finite-size scaling analysis of isotherm curves. One can see that all the curves collapse onto a single function except at high B. The deviation of scaling at high B could probably be due to the presence of weak localization dominating at high B, which causes a weak increase in resistance with increasing B [39]. This can be seen in the R_s-B curves, which show that above B_c, the resistance tends to saturate at high B. Interestingly, the same exponent product $\nu z = 1.4$ is obtained at three different V_G's. The νz observed here is consistent with classical percolation theory ($\nu z \approx 4/3$) [32,37,40] and is similar to that of the chemically doped sample [21]. Note that for the case of chemical doping, the B-tuned SIT has only been observed in the underdoped sample. In our EDLTs, B-tuned SITs occurred at different doping states, and the same νz was observed. This suggests that B-tuned SITs in the EDLT are governed by the same mechanism at different doping levels.

In the bosonic picture of the SIT the perfect duality between Cooper pairs and vortices predicts that R_c is equal to $R_Q = h/(2e)^2 = 6.45\,\mathrm{k}\Omega$ [11,28,30,31,35,41,42]. The values of $R_c \approx R_Q$ observed in YBCO and LSCO suggest that the SITs are driven by quantum phase fluctuations in the hole-doped cuprates, consistent with the bosonic picture [11,12]. However, in electron-doped PCCO we observed R_c much lower than R_Q in both carrier- and B-tuned SITs. This suggests that there are possible fermionic excitations at finite T contributing to the conduction near the SIT in PCCO [32]. Furthermore, it is found that in the B-induced SIT, R_c shares the same evolution with R_n and decreases with increasing charge carriers [Fig. 5(d)]. Moreover, as is shown in the electric-field-effect-induced phase diagram (Fig. 3), the carrier density at which the SIT occurs in PCCO is higher than that in the hole-doped ones. These observations suggest that fermionic excitations at the insulating side of the SIT may occur in n-type superconducting cuprate phases possibly on account of the higher carrier density compared to the hole-doped system. However, to fully understand the role of fermionic excitations on the SIT of electron-doped cuprates further studies will be needed [31,43,44].

To summarize, we investigated carrier- and B-tuned SITs in electron-doped PCCO ultrathin films (see Refs. [45–57]). Using IL as the dielectric material in the EDLTs, the initially insulating states of underdoped PCCO could be gated into superconducting states. In superconducting EDLTs, insulating states were realized by applying B. Through finite-size scaling analysis, it was suggested that carrier- and B-tuned SITs are 2D-QPTs. Moreover, we found the R_c's in PCCO are much lower than R_Q, which probably suggests that there are fermionic excitations at finite T contributing to the conduction near the SIT. The present results could help to further our understanding of quantum criticalities in cuprates.

This work was supported by the Singapore National Research Foundation (NRF) under the Competitive Research Programs (CRP Awards No. NRF-CRP 8-2011-06 and No. NRF-CRP10-2012-02) and the NUS FRC (AcRF Tier 1 Grant No. R-144-000-346-112). P. Yang is supported by the SSLS via NUS Core Support C-380-003-003-001.

[1] C. H. Ahn, A. Bhattacharya, M. Di Ventra, J. N. Eckstein, C. D. Frisbie, M. E. Gershenson, A. M. Goldman, I. H. Inoue, J. Mannhart, A. J. Millis, A. F. Morpurgo, D. Natelson, and J. M. Triscone, Electrostatic modification of novel materials, Rev. Mod. Phys. **78**, 1185 (2006).

[2] K. A. Parendo, K. H. Sarwa, B. Tan, A. Bhattacharya, M. Eblen-Zayas, N. E. Staley, and A. M. Goldman, Electrostatic tuning of the superconductor-insulator transition in two dimensions, Phys. Rev. Lett. **94**, 197004 (2005).

[3] D. Matthey, N. Reyren, J. M. Triscone, and T. Schneider, Electric-field-effect modulation of the transition temperature, mobile carrier density, and in-plane penetration depth of NdBa2Cu3O7-delta thin films, Phys. Rev. Lett. **98**, 057002 (2007).

[4] A. D. Caviglia, S. Gariglio, N. Reyren, D. Jaccard, T. Schneider, M. Gabay, S. Thiel, G. Hammerl, J. Mannhart, and J. M. Triscone, Electric field control of the LaAlO3/SrTiO3 interface ground state, Nature (London) **456**, 624 (2008).

[5] X. X. Xi, C. Doughty, A. Walkenhorst, C. Kwon, Q. Li, and T. Venkatesan, Effects of field-induced hole-density modulation on normal-state and superconducting transport in $YBa_2Cu_3O_{7-x}$, Phys. Rev. Lett. **68**, 1240 (1992).

[6] H. T. Yuan, H. Shimotani, A. Tsukazaki, A. Ohtomo, M. Kawasaki, and Y. Iwasa, High-density carrier accumulation in ZnO field-effect transistors gated by electric double layers of ionic liquids, Adv. Funct. Mater. **19**, 1046 (2009).

[7] K. Ueno, S. Nakamura, H. Shimotani, A. Ohtomo, N. Kimura, T. Nojima, H. Aoki, Y. Iwasa, and M. Kawasaki, Electric-field-induced superconductivity in an insulator, Nature Mater. **7**, 855 (2008).

[8] J. T. Ye, S. Inoue, K. Kobayashi, Y. Kasahara, H. T. Yuan, H. Shimotani, and Y. Iwasa, Liquid-gated interface superconductivity on an atomically flat film, Nature Mater. **9**, 125 (2010).

[9] K. Ueno, S. Nakamura, H. Shimotani, H. T. Yuan, N. Kimura, T. Nojima, H. Aoki, Y. Iwasa, and M. Kawasaki, Discovery of superconductivity in KTaO3 by electrostatic carrier doping, Nat. Nanotechnol. **6**, 408 (2011).

[10] Y. Yamada, K. Ueno, T. Fukumura, H. T. Yuan, H. Shimotani, Y. Iwasa, L. Gu, S. Tsukimoto, Y. Ikuhara, and M. Kawasaki, Electrically induced ferromagnetism at room temperature in cobalt-doped titanium dioxide, Science **332**, 1065 (2011).

[11] A. T. Bollinger, G. Dubuis, J. Yoon, D. Pavuna, J. Misewich, and I. Bozovic, Superconductor-insulator transition in La2-xSrxCuO4 at the pair quantum resistance, Nature (London) **472**, 458 (2011).

[12] X. Leng, J. Garcia-Barriocanal, S. Bose, Y. Lee, and A. M. Goldman, Electrostatic control of the evolution from a superconducting phase to an insulating phase in ultrathin YBa2CaCu3O7-x films, Phys. Rev. Lett. **107**, 027001 (2011).

[13] J. Garcia-Barriocanal, A. Kobrinskii, X. Leng, J. Kinney, B. Yang, S. Snyder, and A. M. Goldman, Electronically driven superconductor-insulator transition in electrostatically doped La2CuO4+delta thin films, Phys. Rev. B **87**, 024509 (2013).

[14] A. S. Dhoot, S. C. Wimbush, T. Benseman, J. L. MacManus-Driscoll, J. R. Cooper, and R. H. Friend, Increased Tc in Electrolyte-Gated Cuprates, Adv. Mater. **22**, 2529 (2010).

[15] J. T. Ye, Y. J. Zhang, R. Akashi, M. S. Bahramy, R. Arita, and Y. Iwasa, Superconducting dome in a gate-tuned band insulator, Science **338**, 1193 (2012).

[16] M. Nakano, K. Shibuya, D. Okuyama, T. Hatano, S. Ono, M. Kawasaki, Y. Iwasa, and Y. Tokura, Collective bulk carrier delocalization driven by electrostatic surface charge accumulation, Nature (London) **487**, 459 (2012).

[17] J. Jeong, N. Aetukuri, T. Graf, T. D. Schladt, M. G. Samant, and S. S. P. Parkin, Suppression of metal-insulator transition in VO2 by electric field-induced oxygen vacancy formation, Science **339**, 1402 (2013).

[18] X. Leng, J. Garcia-Barriocanal, J. Kinney, B. Y. Yang, Y. Lee, and A. M. Goldman, Electrostatic tuning of the superconductor to insulator transition of $YBa_2Cu_3O_{7-x}$ using ionic liquids, J. Phys.: Conf. Ser. **449**, 012009 (2013).

[19] N. P. Armitage, P. Fournier, and R. L. Greene, Progress and perspectives on electron-doped cuprates, Rev. Mod. Phys. **82**, 2421 (2010).

[20] G. T. Seidler, T. F. Rosenbaum, and B. W. Veal, 2-dimensional superconductor-insulator transition in bulk single-crystal YBa2Cu3O6.38, Phys. Rev. B **45**, 10162 (1992).

[21] S. Tanda, S. Ohzeki, and T. Nakayama, Bose-glass vortex-glass phase-transition and dynamic scaling for high-Tc Nd2-xCexCuO4 thin-films, Phys. Rev. Lett. **69**, 530 (1992).

[22] S. Smadici, J. C. T. Lee, S. Wang, P. Abbamonte, G. Logvenov, A. Gozar, C. D. Cavellin, and I. Bozovic, Superconducting transition at 38 K in insulating-overdoped La2CuO4-La1.64Sr0.36CuO4 superlattices: Evidence for interface electronic redistribution from resonant soft x-Ray scattering, Phys. Rev. Lett. **102**, 107004 (2009).

[23] See Supplemental Material Sec. 2 at http://link.aps.org/supplemental/10.1103/PhysRevB.92.020503 for testing device reversibility.

[24] See Supplemental Material Sec. 4 at http://link.aps.org/supplemental/10.1103/PhysRevB.92.020503 for the measurement of *R*-*T* curves at various magnetic fields, Sec. 5 for testing the reproducibility of the EDLT experiments, and Sec. 6 for the discussion of insulating behavior near the SIT.

[25] K. Jin, P. Bach, X. H. Zhang, U. Grupel, E. Zohar, I. Diamant, Y. Dagan, S. Smadici, P. Abbamonte, and R. L. Greene, Anomalous enhancement of the superconducting transition temperature of electron-doped La2-xCexCuO4 and $Pr_{2-x}Ce_xCuO_4$ cuprate heterostructures, Phys. Rev. B **83**, 060511 (2011).

[26] See Supplemental Material Sec. 3 at http://link.aps.org/supplemental/10.1103/PhysRevB.92.020503 for a detailed estimation of carrier concentration.

[27] J. L. Peng, E. Maiser, T. Venkatesan, R. L. Greene, and G. Czjzek, Concentration range for superconductivity in high-quality $Pr_{2-x}Ce_xCuO_4$-y thin films, Phys. Rev. B **55**, R6145(R) (1997).

[28] M. P. A. Fisher, Quantum phase-transitions in disordered 2-dimensional superconductors, Phys. Rev. Lett. **65**, 923 (1990).

[29] S. L. Sondhi, S. M. Girvin, J. P. Carini, and D. Shahar, Continuous quantum phase transitions, Rev. Mod. Phys. **69**, 315 (1997).

[30] V. F. Gantmakher and V. T. Dolgopolov, Superconductor-insulator quantum phase transition, Phys.-Usp. **53**, 1 (2010).

[31] A. M. Goldman and N. Markovic, Superconductor-insulator transitions in the two-dimensional limit, Phys. Today **51**(11), 39 (1998).

[32] A. Yazdani and A. Kapitulnik, Superconducting-insulating transition in 2-dimensional alpha-moge thin-films, Phys. Rev. Lett. **74**, 3037 (1995).

[33] Y. Liu, K. A. McGreer, B. Nease, D. B. Haviland, G. Martinez, J. W. Halley, and A. M. Goldman, Scaling of the insulator-to-superconductor transition in ultrathin amorphous Bi films, Phys. Rev. Lett. **67**, 2068 (1991).

[34] N. Markovic, C. Christiansen, A. M. Mack, W. H. Huber, and A. M. Goldman, Superconductor-insulator transition in two dimensions, Phys. Rev. B **60**, 4320 (1999).

[35] M. A. Steiner, N. P. Breznay, and A. Kapitulnik, Approach to a superconductor-to-Bose-insulator transition in disordered films, Phys. Rev. B **77**, 212501 (2008).

[36] D. H. Lee, Z. Q. Wang, and S. Kivelson, Quantum percolation and plateau transitions in the quantum hall-effect, Phys. Rev. Lett. **70**, 4130 (1993).

[37] Y. Dubi, Y. Meir, and Y. Avishai, Unifying model for several classes of two-dimensional phase transition, Phys. Rev. Lett. **94**, 156406 (2005).

[38] R. Schneider, A. G. Zaitsev, D. Fuchs, and H. von Lohneysen, Superconductor-Insulator Quantum Phase Transition in Disordered FeSe Thin Films, Phys. Rev. Lett. **108**, 257003 (2012).

[39] A. Kussmaul, J. S. Moodera, P. M. Tedrow, and A. Gupta, 2-dimensional character of the magnetoresistance in Nd1.85Ce0.15CuO4-delta thin-films, Physica C **177**, 415 (1991).

[40] N. Mason and A. Kapitulnik, Dissipation effects on the superconductor-insulator transition in 2D superconductors, Phys. Rev. Lett. **82**, 5341 (1999).

[41] D. B. Haviland, Y. Liu, and A. M. Goldman, Onset of superconductivity in the two-dimensional limit, Phys. Rev. Lett. **62**, 2180 (1989).

[42] A. F. Hebard and M. A. Paalanen, Magnetic-field-tuned superconductor-insulator transition in 2-dimensional films, Phys. Rev. Lett. **65**, 927 (1990).

[43] S. Dukan and Z. Tesanovic, Superconductivity in a high magnetic-field - excitation spectrum and tunneling properties, Phys. Rev. B **49**, 13017 (1994).

[44] H. Aubin, C. A. Marrache-Kikuchi, A. Pourret, K. Behnia, L. Berge, L. Dumoulin, and J. Lesueur, Magnetic-field-induced quantum superconductor-insulator transition in Nb0.15Si0.85, Phys. Rev. B **73**, 094521 (2006).

[45] M. Brinkmann, T. Rex, H. Bach, and K. Westerholt, Extended superconducting concentration range observed in $Pr_{2-X}Ce_xCuO_{4-Delta}$, Phys. Rev. Lett. **74**, 4927 (1995).

[46] Y. Krockenberger, J. Kurian, A. Winkler, A. Tsukada, M. Naito, and L. Alff, Superconductivity phase diagrams for the electron-doped cuprates R(2-x)Ce(x)CuO(4) (R = La, Pr, Nd, Sm, and Eu), Phys. Rev. B **77**, 060505 (2008).

[47] O. Matsumoto, A. Utsuki, A. Tsukada, H. Yamamoto, T. Manabe, and M. Naito, Synthesis and properties of superconducting T-'-R2CuO4 (R = Pr, Nd, Sm, Eu, Gd), Phys. Rev. B **79**, 100508 (2009).

[48] P. Fournier, J. Higgins, H. Balci, E. Maiser, C. J. Lobb, and R. L. Greene, Anomalous saturation of the phase coherence length in underdoped $Pr_{2-x}Ce_xCuO_4$ thin films, Phys. Rev. B **62**, R11993(R) (2000).

[49] T. Sekitani, M. Naito, and N. Miura, Kondo effect in underdoped n-type superconductors, Phys. Rev. B **67**, 174503 (2003).

[50] F. Rullier-Albenque, H. Alloul, and R. Tourbot, Disorder and transport in cuprates: Weak localization and magnetic contributions, Phys. Rev. Lett. **87**, 157001 (2001).

[51] Y. Dagan, M. C. Barr, W. M. Fisher, R. Beck, T. Dhakal, A. Biswas, and R. L. Greene, Origin of the anomalous low temperature upturn in the resistivity of the electron-doped cuprate superconductors, Phys. Rev. Lett. **94**, 057005 (2005).

[52] M. Z. Cieplak, A. Malinowski, S. Guha, and M. Berkowski, Localization and interaction effects in strongly underdoped La2-xSrxCuO4, Phys. Rev. Lett. **92**, 187003 (2004).

[53] S. Finkelman, M. Sachs, G. Droulers, N. P. Butch, J. Paglione, P. Bach, R. L. Greene, and Y. Dagan, Resistivity at low temperatures in electron-doped cuprate superconductors, Phys. Rev. B **82**, 094508 (2010).

[54] Y. Onose, Y. Taguchi, K. Ishizaka, and Y. Tokura, Charge dynamics in underdoped Nd(2-x)Ce(x)CuO(4): Pseudogap and related phenomena, Phys. Rev. B **69**, 024504 (2004).

[55] E. M. Motoyama, G. Yu, I. M. Vishik, O. P. Vajk, P. K. Mang, and M. Greven, Spin correlations in the electron-doped high-transition-temperature superconductor Nd2-xCexCuO4 +/-delta, Nature (London) **445**, 186 (2007).

[56] Y. Dagan, M. M. Qazilbash, C. P. Hill, V. N. Kulkarni, and R. L. Greene, Evidence for a quantum phase transition in Pr2-xCexCuO4-delta from transport measurements, Phys. Rev. Lett. **92**, 167001 (2004).

[57] F. F. Balakirev, J. B. Betts, A. Migliori, I. Tsukada, Y. Ando, and G. S. Boebinger, Quantum phase transition in the magnetic-field-induced normal state of optimum-doped high-T-c cuprate superconductors at low temperatures, Phys. Rev. Lett. **102**, 017004 (2009).